UPDATED TOOL PATH MODELLING WITH PERIODIC DELAY FOR CHATTER PREDICTION IN MILLING.

Ronald Faassen
Department of Mechanical Engineering
Eindhoven University of Technology
Netherlands
r.p.h.faassen@tue.nl

Nathan van de Wouw
Department of Mechanical Engineering
Eindhoven University of Technology
Netherlands
n.v.d.wouw@tue.nl

Han Oosterling
Industrial Prototyping
TNO Science and Industry
Netherlands
han.oosterling@tno.nl

Henk Nijmeijer
Department of Mechanical Engineering
Eindhoven University of Technology
Netherlands
h.nijmeijer@tue.nl

Abstract

The efficiency of the high speed milling process is often limited by chatter. In order to predict the occurrence of chatter, accurate models are necessary. In most models regarding milling, the cutter is assumed to follow a circular tooth path. However, the real tool path is trochoidal in an ideal case, i.e. without vibrations of the tool. Therefore, models using a circular tool path lead to errors, especially when the cutting angle is close to 0 or π radians. An updated model for the milling process is presented which features an updated model of the undeformed chip thickness and a time-periodic delay. Furthermore, the stability of the milling system, and hence the occurrence of chatter, is investigated using the traditional and the new model by means of the semi-discretization method. Especially for low immersion cuts, the stability lobes diagram (SLD) using the updated model shows significant differences compared to the SLD using the traditional model.

Key words

High-speed milling, time-delay, stability, chip thickness, tool path, DDE.

1 Introduction

High speed milling is used in many sectors of industry. For example in the aerospace manufacturing industry, large parts are made out of a single workpiece where 90% of the material is removed. Moreover, in the mould making industry high speed milling is used. Here, as a rule the radial immersion is low as a result of the complex geometries of the workpiece and the difficult machinability of the workpiece material. The material removal rate in milling is often limited by the occurrence of an instability phenomenon called regenerative chatter. Chatter results in heavy vibrations of the tool causing an inferior workpiece surface quality, rapid tool wear and noise.

Research regarding regenerative chatter started in the late 1950's with (Tlusty and Polacek, 1963) and (Tobias and Fishwick, 1958). They introduced a stability lobes diagram (SLD), which graphically shows the stability limit as a function of machining parameters, such as spindle speed and depth of cut. The stability of the milling process for low immersion cutting was investigated recently in (Davies *et al.*, 2002; Insperger and Stépán, 2004*c*; Szalai *et al.*, 2004). They focussed on the impact behaviour of the tool hitting the workpiece for a small period of time.

In most models regarding milling, see e.g. (Insperger *et al.*, 2003; Altintas, 2000), the tooth path is modelled as a circular arc. We will call this tooth path model the traditional model in this paper. Using this model, the undeformed chip thickness is approximated by a sinusoid. However, the path of a milling cutter is trochoidal (Martellotti, 1941; Martellotti, 1945), which leads to different equations for the undeformed chip thickness. More accurate models exist compared to the sinusoidal approximation (Spiewak, 1994; Spiewak, 1995; Li *et al.*, 2001), but they are not used widely, because of the complex equations involved. However, especially when $\sin\phi(t)$ is small (with $\phi(t)$ the tooth angle at time t), which is often the case in low immersion cutting, the errors using the traditional model are large. Furthermore, using the traditional model it is assumed that for upmilling the entry angle of the cut is $\phi_s = 0$ rad and that the exit angle for downmilling is $\phi_e = \pi$ rad. Using a new model for the static chip thickness also shows that the tool enters the cut somewhat sooner and

leaves it somewhat later.

For the prediction of chatter in high speed milling, not only the static chip thickness is important, but also the dynamic chip thickness, which is due to the regenerative effect. Most often, the dynamic chip thickness is calculated by subtracting the vibrations at the current time $\underline{v}(t)$ and the time one tooth passing time earlier $\underline{v}(t-\hat{\tau})$, see e.g. (Altintas, 2000; Szalai *et al.*, 2004; Insperger and Stépán, 2004*b*; Altintas and Budak, 1995). This results in a delay differential equation (DDE) modelling the milling process. However, we will show that the delay is not constant, but periodic when the trochoidal tool path is taken into account.

In this paper, a new model for the milling process is presented, in which the tool path is described by a trochoid. Hereto, a new equation describing the static chip thickness is derived. Furthermore, the delay is modelled as being periodic instead of constant and new equations for the entry and exit angles are formulated. Using this new model, the stability limit is found using the semi-discretization method (Insperger and Stépán, 2004*a*; Insperger and Stépán, 2004*b*). Especially for low immersion cutting, it appears that the stability lobes change drastically using the new model compared with the lobes generated using the traditional model.

The paper is organized as follows: in section 2, the new equations describing the undeformed chip thickness, the delay and the entry and exit angles are derived and a comparison between different models is provided. In section 3, the stability of the new and the traditional model is investigated using the semi-discretization method and discussed in terms of the implication for the milling process in section 4. Finally, conclusions are drawn in section 5.

2 Modelling the milling process

The undeformed chip thickness is the sum of the static chip thickness $h_{j,\mathsf{stat}}(t)$ and the dynamic chip thickness $h_{j,\mathsf{dyn}}(t)$. The static chip thickness is the chip thickness if no vibrations of the cutter would occur and the dynamic chip thickness is the part which is a result of the vibrations of the cutter:

$$h_j(t) = h_{j,\mathsf{stat}}(t) + h_{j,\mathsf{dyn}}(t). \tag{1}$$

For a 2-dimensional case, the static chip thickness is often modelled by

$$h_{j,\mathsf{stat}}(t) = f_z \sin\phi_j(t), \tag{2}$$

where $h_{j,\mathsf{stat}}(t)$ is the undeformed chip thickness if no vibrations of the cutter occur, f_z is the chip load and $\phi_j(t)$ is the angle of tooth j at time t. The dynamic chip thickness is often modelled by

$$h_{j,\mathsf{dyn}}(t) = \left[\sin\phi_j(t)\ \cos\phi_j(t)\right]\left(\underline{v}(t) - \underline{v}(t-\hat{\tau})\right). \tag{3}$$

Here the constant time delay is given by

$$\hat{\tau} = \frac{2\pi}{z\Omega}, \tag{4}$$

where z is the number of teeth and Ω is the spindle speed in rad/s.

This model assumes a circular tooth path. However, the real tool path is trochoidal, see figure 1. In this figure, the chip load is chosen rather unrealistically large to increase readability of the figure. The tool moves in the feed direction x. The meaning of the points defined in the figure are shown in table 1. In figure 2, the circular tool path approximation is shown.

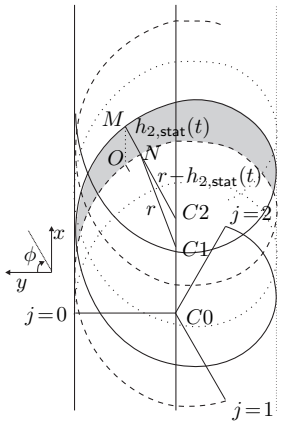

Figure 1: The tooth path of a mill with three teeth.

Table 1: Positions of points of figure 1.

Point	Position
$C0$	$\underline{p}_c(t=0)$
$C1$	$\underline{p}_c(t-\tau_2(t))$
$C2$	$\underline{p}_c(t)$
M	$\underline{p}_2(t)$
N	$\underline{p}_1(t-\tau_2(t))$
O	$\underline{p}_1(t-\hat{\tau})$

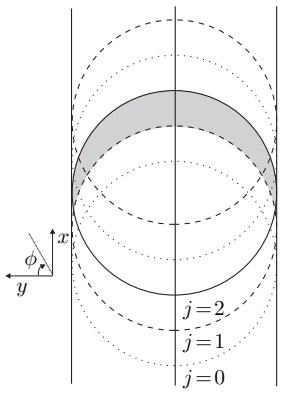

Figure 2: The circular tooth path approximation of a mill with three teeth.

The delay $\tau_j(t)$ is defined as the delay that is involved when calculating the chip thickness that tooth j removes at time t. In figure 1, τ_2 is the difference between the time when tooth 2 was at point M and tooth 1 was at point N. Here, the index 2 refers to tooth 2, since this delay is involved when calculating the dynamic chip thickness experienced by tooth 2 at time t.

The centre of the cutter at time t is at position $C2$. At time $t-\tau_2$, the centre is at position $C1$. Note that when applying (3) with a constant delay $\hat{\tau}$, the vibrations at point O are subtracted from the vibrations at point M. However, the dynamic chip thickness is described by the subtraction of the vibrations at point N from the vibrations of point M.

In the sequel, an equation for the static chip thickness is derived for the case of a trochoidal tool path. By doing so, also an expression for the delay is obtained, which can be used to calculate the dynamic chip thickness in a later stage. It should be noted that the vibrations of the cutter are assumed zero for deriving the delay. When vibrations of the tool are taken into account, points M and N move as a result of these vibrations. Hence, also the delay changes and becomes state-dependent. However, for the sake of simplicity, this is not taken into account here.

The position of a point $\underline{p}_j(t)$ on the tip of tooth j at time t can be described as the sum of the position of the centre of the cutter $\underline{p}_c(t) = \left[\frac{f_z z}{2\pi}\phi_0(t)\ 0\right]^T$ at time t and the position of the tip relative to this centre. With $\underline{p}_j = \left[p_{x_j}\ p_{y_j}\right]^T$, this gives

$$\begin{aligned}\underline{p}_j(t) &= \underline{p}_c(t) + \begin{bmatrix} r\sin\phi_j(t) \\ r\cos\phi_j(t)\end{bmatrix} \\ &= \begin{bmatrix} \frac{f_z z}{2\pi}\phi_0(t) + r\sin\phi_j(t) \\ r\cos\phi_j(t)\end{bmatrix},\end{aligned} \tag{5}$$

with r the radius of the tool. Here a constant spindle speed Ω and feed per tooth f_z are assumed.

Point N in figure 1 can be described as the position of tooth 1 at time $t-\tau_2(t)$.

$$\begin{aligned}&\underline{p}_1\big(t-\tau_2(t)\big) = \\ &\begin{bmatrix} \frac{f_z z}{2\pi}\phi_0\big(t-\tau_2(t)\big) + r\sin\phi_1\big(t-\tau_2(t)\big) \\ r\cos\phi_1\big(t-\tau_2(t)\big)\end{bmatrix}.\end{aligned} \tag{6}$$

However, it can also be defined as the position of tooth 2 at time t for a tool radius of $r - h_{2,\mathsf{stat}}(t)$.

$$\underline{p}_{2*}(t) = \begin{bmatrix} \frac{f_z z}{2\pi}\phi_0(t) + \big(r - h_{2,\mathsf{stat}}(t)\big)\sin\phi_2(t) \\ \big(r - h_{2,\mathsf{stat}}(t)\big)\cos\phi_2(t)\end{bmatrix}. \tag{7}$$

Equating (6) to (7) in y-direction and generalizing for an arbitrary tooth j gives

$$r\cos\phi_{j-1}\big(t-\tau_j(t)\big) = \big(r - h_{j,\mathsf{stat}}(t)\big)\cos\phi_j(t). \tag{8}$$

After substitution of

$$\phi_j(t) = \phi_0(t) - j\theta = \Omega t - j\frac{2\pi}{z}, \tag{9}$$

with θ the angle between two subsequent teeth

$$\theta = \frac{2\pi}{z} = \hat{\tau}\Omega, \tag{10}$$

the chip thickness can be expressed as

$$\begin{aligned}h_{j,\mathsf{stat}}(t) &= \frac{r\cos\phi_j(t) - r\cos\Big(\phi_j\big(t-\tau_j(t)\big)+\theta\Big)}{\cos\phi_j(t)} \\ &:= \frac{A}{\cos\phi_j(t)} = h_y.\end{aligned} \tag{11}$$

Similarly, by equating (6) to (7) in x-direction and generalizing for an arbitrary tooth j, another expression for the chip thickness is found

$$\begin{aligned}&h_{j,\mathsf{stat}}(t) \\ &= \frac{\frac{f_z z}{2\pi}\Omega\tau_j(t) + r\sin\phi_j(t) - r\sin\Big(\phi_j\big(t-\tau_j(t)\big)+\theta\Big)}{\sin\phi_j(t)} \\ &:= \frac{B}{\sin\phi_j(t)} = h_x.\end{aligned} \tag{12}$$

Now, (11) and (12) can be used to express the chip thickness. However, if the denominator of any of these equations approaches zero, the equation tends to $\pm\infty$. Therefore, it will be shown that both equations can be combined to obtain a single equation for the chip thickness that can always be used. Before this expression for the chip thickness can be formulated, first an expression for the time-varying delay should be derived.

2.1 Time delay

Setting $h_{j,\mathsf{stat}}(t) = h_y = h_x$, and using (11) and (12) gives:

$$\frac{A}{\cos\phi_j(t)} = \frac{B}{\sin\phi_j(t)} \Rightarrow B\cos\phi_j(t) = A\sin\phi_j(t). \tag{13}$$

Substitution of (11), (12), (4) and (9) in (13) and applying trigonometric relations yields

$$\frac{f_z\tau_j(t)}{\hat{\tau}}\cos\phi_j(t) + r\sin\Big(\Omega\big(\tau_j(t)-\hat{\tau}\big)\Big) = 0. \tag{14}$$

The time-varying delay can be regarded as the sum of the constant tooth passing time delay $\hat{\tau}$ and a small time-periodic function $\delta\tau_j(t)$.

$$\tau_j(t) = \hat{\tau} + \delta\tau_j(t), \tag{15}$$

with $\delta\tau_j(t+\hat{\tau}) = \delta\tau_{j-1}(t)$. Substitution of (15) in (14) gives

$$f_z\cos\phi_j(t) + \frac{f_z\cos\phi_j(t)}{\hat{\tau}}\delta\tau_j(t) + r\sin\big(\Omega\delta\tau_j(t)\big) = 0. \tag{16}$$

Since $\Omega\delta\tau_j(t) \ll 1$, truncation of the Taylor's series expansion of $\sin\big(\Omega\delta\tau_j(t)\big)$ after the first-order term yields $\sin\big(\Omega\delta\tau_j(t)\big) \approx \Omega\delta\tau_j(t)$. Using this approximation in (16) gives an expression for $\delta\tau_j(t)$:

$$\delta\tau_j(t) = -\frac{\hat{\tau} f_z \cos\phi_j(t)}{f_z \cos\phi_j(t) + r\Omega\hat{\tau}}. \tag{17}$$

The time-varying delay can now be expressed by substituting (10) and (17) in (15) and rearranging terms as

$$\tau_j(t) = \frac{\hat{\tau}\theta r}{f_z \cos\phi_j(t) + \theta r}. \tag{18}$$

2.2 Chip thickness

Since the time-varying delay is now known, an expression for the chip thickness can be derived. The chip thickness can be expressed either by (11) or (12). However, both expressions can not be used when the denominator becomes zero. Therefore, by adding these two expressions with an appropriate weighting function an appropriate expression is found:

$$h_{j,\mathsf{stat}}(t) = h_x \sin^2\phi_j(t) + h_y \cos^2\phi_j(t), \tag{19}$$

which holds, since $\sin^2\phi_j(t) + \cos^2\phi_j(t) = 1$ and $h_{j,\mathsf{stat}}(t) = h_x = h_y$. Substitution of (11) and (12) in (19) and applying trigonometric relations and subsequently using (9) and (4) yields

$$h_{j,\mathsf{stat}}(t) = r - r\cos\big(\Omega\tau_j(t) - \theta\big) + \frac{f_z}{\hat{\tau}}\tau_j(t)\sin\phi_j(t). \tag{20}$$

Substitution of (18) in (20) and rearranging terms gives an expression for the static chip thickness

$$\begin{aligned} h_{j,\mathsf{stat}}(t) = r - r\cos\left(\frac{\theta f_z \cos\phi_j(t)}{f_z\cos\phi_j(t) + \theta r}\right) \\ + \left(\frac{f_z\theta r}{f_z\cos\phi_j(t) + \theta r}\right)\sin\phi_j(t). \end{aligned} \tag{21}$$

If the time-varying delay is not considered, i.e. $\tau_j(t) := \hat{\tau}$, expression (21) equals equation (2).

2.3 Start and exit angles

For a full immersion cut, the start angle is usually defined as $\phi_s = 0$ rad and the exit angle as $\phi_e = \pi$ rad. However, the tool enters the cut somewhat earlier (i.e. $\phi_s < 0$) and leaves the cut somewhat later (i.e. $\phi_e > \pi$). This can be shown using the definition of the chip thickness of equation (11). At the start and exit angles the chip thickness is zero, which gives

$$h_y = \frac{r\cos\phi_j(t) - r\cos\Big(\phi_j\big(t - \tau_j(t)\big) + \theta\Big)}{\cos\phi_j(t)} = 0. \tag{22}$$

Using (9) this can also be expressed as

$$\frac{r\cos\phi_j(t) - r\cos\big(\phi_j(t) - \Omega\tau_j(t) + \theta\big)}{\cos\phi_j(t)} = 0. \tag{23}$$

This is true if the numerator is zero. This gives two possible solutions of (23):

$$-\Omega\tau_j(t) + \theta = 2k\pi, \tag{24}$$

$$\phi_j(t) - \Omega\tau_j(t) + \theta = -\phi_j(t) + 2k\pi, \tag{25}$$

with $k = 0, 1, 2, \ldots$. Substituting (18) in (24) and rearranging terms gives

$$\frac{\theta f_z \cos\phi_j(t)}{f_z\cos\phi_j(t) + \theta r} = 2k\pi. \tag{26}$$

This does not lead to angles close to 0 or π radians (e.g. $\phi = 0.5\pi$ is a solution). Substituting (18) in (25) and rearranging terms gives

$$\frac{\theta f_z \cos\phi_j(t)}{f_z\cos\phi_j(t) + \theta r} = -2\phi_j(t) + 2k\pi. \tag{27}$$

This equation can not be solved analytically. Therefore, equation (27) is approximated using Taylor's series.

For a full immersion cut, the entry angle can be described by $\phi_s = 0 + \delta\phi_s = \delta\phi_s$. Applying Taylor's series $(\cos\delta\phi_s \approx 1)$ to equation (27), for $k = 0$, the entry angle ϕ_s can be approximated by

$$\phi_s = \delta\phi_s \approx -\frac{\theta f_z}{2(f_z + \theta r)}. \tag{28}$$

For a full immersion cut, the exit angle can be described by $\phi_e = \phi_j(t) = \pi + \delta\phi_e$. Applying Taylor's series, $(\cos(\pi + \delta\phi_e) \approx -1)$ to equation (27), for $k = 1$, the exit angle ϕ_e can be approximated by

$$\phi_e = \pi + \delta\phi_e \approx \pi - \frac{\theta f_z}{2(f_z - \theta r)}. \tag{29}$$

2.4 Results of the tool path model

In the new model, in contrast with the traditional model (2), the static chip thickness is described by (21). The delay which is traditionally assumed constant is updated using the periodic function (18). Finally, the entry and exit angles are described by (28) and (29), respectively.

For verification purposes, the approximative model for the chip thickness (21) is compared to the chip thickness computed numerically using an optimization function. For this numerical computation, first the delay is computed numerically by minimizing the absolute value of the left hand side of (14) via a constrained optimization function with the boundary condition $0.75\hat{\tau} \leq \tau_j(t) \leq 1.25\hat{\tau}$. This delay is substituted

in (20) to calculate the chip thickness. The resulting chip thickness is compared to the chip thickness using the circular tooth path of equation (2), the new model, and the models of (Martellotti, 1941) and (Li *et al.*, 2001). In (Martellotti, 1941) the chip thickness is approximated by

$$h_{j,\text{stat}}(t) = r + f_z \sin(\phi_j(t)) - \sqrt{r^2 - f_z^2 \cos^2 \phi_j(t)}. \tag{30}$$

In (Li *et al.*, 2001) the chip thickness is approximated by

$$h_{j,\text{stat}}(t) = r \left(1 - \left(1 - \frac{2 f_z \sin \phi_j(t)}{r + \frac{z f_z}{2\pi} \cos \phi_j(t)} - \frac{f_z^2 \cos 2\phi_j(t)}{\left(r + \frac{z f_z}{2\pi} \cos \phi_j(t) \right)^2} + \frac{f_z^3 \sin \phi_j(t) \cos^2 \phi_j(t)}{\left(r + \frac{z f_z}{2\pi} \cos \phi_j(t) \right)^3} \right)^{1/2} \right) \tag{31}$$

In figure 3 the chip thickness is shown for $r = 5$ mm and $z = 2$ and a rather unrealistic chip load $f_z = 2$ mm/tooth. This value is chosen to magnify the differences between the various models for visualization purposes. The new model and the model of Li *et al.* fit

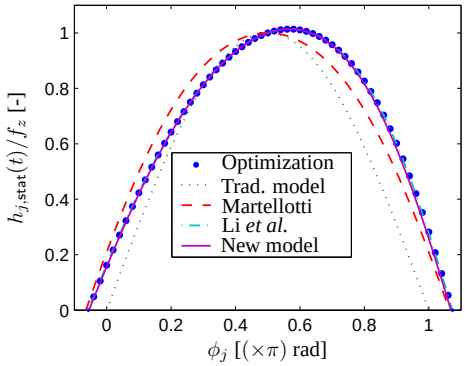

Figure 3: Chip thickness as a function of rotation angle for various models; $r = 5$ mm, $z = 2$, $f_z = 2$ mm/tooth.

the numerical results very well. It can be seen that the chip thickness function does not have a symmetry axis at $\phi = 0.5\pi$. However, the model of Martellotti and the traditional model do have this symmetry axis. Furthermore, the maximum chip thickness is larger than the chip load f_z according to the numerical results. This is also predicted by the model of Li *et al.* and the proposed new model, whereas the traditional and the Martellotti model do not predict this.

The errors of the chip thickness of the various models relative to the numerically computed chip thickness are shown in figure 4. Here a more realistic case of $f_z = 0.2$ mm/tooth is taken. Herein, the differences between the models are clearly visible. Especially when

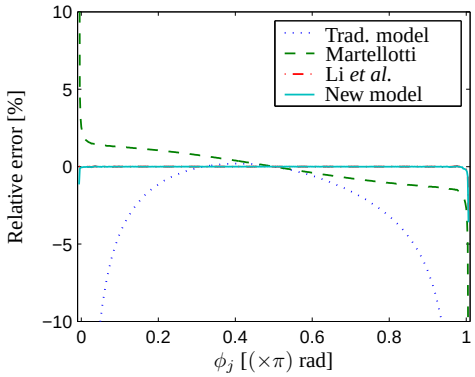

Figure 4: Relative error in chip thickness as a function of rotation angle for various models; $r = 5$ mm, $z = 2$, $f_z = 0.2$ mm/tooth.

the chip thickness is small, the relative error becomes very large for both the traditional model and the model of Martellotti. For the new model and the model of Li *et al.* the errors are rather small. The drawback of the model by (Li *et al.*, 2001) is that is does not give an expression for the delay.

The start and exit angles according to (28) and (29) are shown in figure 5 for the case where $f_z = 0.2$ mm/tooth. The results of the various models, shown in figure 3, are also treated in this figure. The

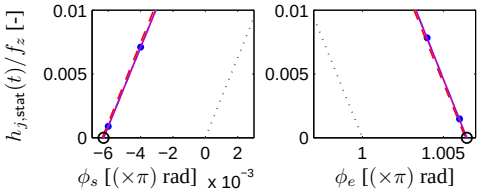

Figure 5: Entry (left) and exit (right) angles. The values from (28) and (29) are plotted as circles; $r = 5$ mm, $z = 2$, $f_z = 0.2$ mm/tooth. For legend, see figure 3.

expressions that are found for the entry and exit angles match very well with the angles where the chip thickness of the new model is zero.

The delay expressed by equation (18) is compared to the delay calculated numerically using the optimization function. The results can be seen in figure 6. Results of the proposed model fit the numerical results very well. For small angles, the delay is smaller than the constant $\hat{\tau}$. This is the situation shown in figure 1 where point O is the point at $t-\hat{\tau}$ and point N the point at $t-\tau_2$. When cutting, the tooth reaches point O sooner than point N and hence $\tau_j(t) < \hat{\tau}$. If $0.5\pi < \phi_j(t) < \phi_e$, the delay becomes larger than $\hat{\tau}$. Then point O' is reached later than point N', where the prime symbolizes the new position of points O and N.

The relative error of both the time delay and chip thickness of the traditional model increases as the chip thickness becomes smaller. Since the chip thickness is

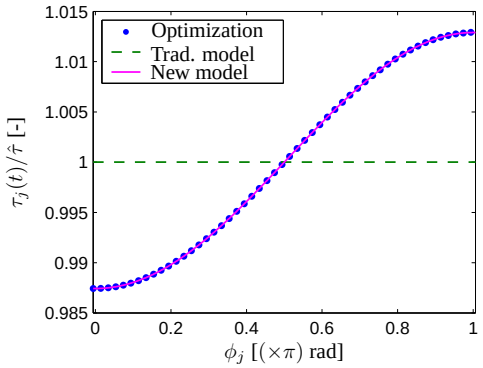

Figure 6: Normalized delay as a function of rotation angle; $r = 5$ mm, $z = 2$, $f_z = 0.2$ mm/tooth.

very small in low immersion cutting, it is likely that the use of the traditional model leads to errors for this type of cuts. Therefore, in section 3, the stability of milling models using both tooth path models is investigated. In the next section, the milling model is presented.

2.5 The milling system

A schematic representation of the milling process is shown in figure 7 and a block diagram of the model is shown in figure 8.

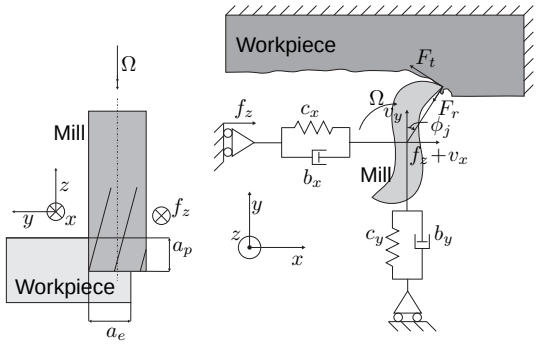

Figure 7: Schematic representation of the milling process.

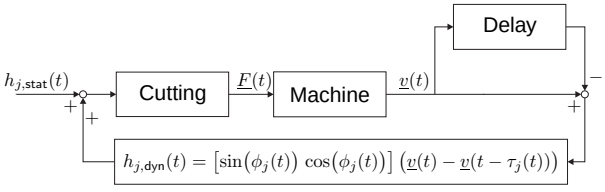

Figure 8: Block diagram of the milling process.

The dynamics of the machine are represented as a 2DOF mass-spring-damper system in figure 7. For representing general linear dynamics, a state-space formulation is used:

$$\begin{aligned} \dot{\underline{z}}(t) &= \mathbf{A}\underline{z}(t) + \mathbf{B}u(t), \\ y(t) &= \mathbf{C}\underline{z}(t) + \mathbf{D}u(t). \end{aligned} \tag{32}$$

These equations describe the relation between the input u of a system (in our case the force that acts on the mill $\underline{F}$) and the output y of this system (in our case the displacement of the mill $\underline{v}$).

Since in the milling equations both the x- and y-directions are necessary (each with its own dynamics), the state vectors of these two directions are first assembled in a single state vector as follows:

$$\begin{aligned} \dot{\underline{z}} &= \begin{bmatrix} \dot{\underline{z}}_x \\ \dot{\underline{z}}_y \end{bmatrix} = \begin{bmatrix} \mathbf{A}_x & \mathbf{0} \\ \mathbf{0} & \mathbf{A}_y \end{bmatrix} \begin{bmatrix} \underline{z}_x \\ \underline{z}_y \end{bmatrix} + \begin{bmatrix} \mathbf{B}_x & \mathbf{0} \\ \mathbf{0} & \mathbf{B}_y \end{bmatrix} \begin{bmatrix} u_x \\ u_y \end{bmatrix} \\ &= \mathbf{A}\underline{z} + \mathbf{B}\underline{u}, \\ \underline{y} &= \begin{bmatrix} y_x \\ y_y \end{bmatrix} = \begin{bmatrix} \mathbf{C}_x & \mathbf{0} \\ \mathbf{0} & \mathbf{C}_y \end{bmatrix} \begin{bmatrix} \underline{z}_x \\ \underline{z}_y \end{bmatrix} + \begin{bmatrix} \mathbf{D}_x & \mathbf{0} \\ \mathbf{0} & \mathbf{D}_y \end{bmatrix} \begin{bmatrix} u_x \\ u_y \end{bmatrix} \\ &= \mathbf{C}\underline{z} + \mathbf{D}\underline{u}. \end{aligned} \tag{33}$$

Using the new tooth path model has consequences for the blocks Cutting and Delay. The force that acts on the tooth j in tangential and radial direction can be described by (Faassen *et al.*, 2003):

$$\begin{aligned} F_{t_j}(t) &= \big(K_t\, a_p\, h_j(t)^{x_F} + K_{te}\, a_p\big) g_j\big(\phi_j(t)\big), \\ F_{r_j}(t) &= \big(K_r\, a_p\, h_j(t)^{x_F} + K_{re}\, a_p\big) g_j\big(\phi_j(t)\big), \end{aligned} \tag{34}$$

where $0 < x_F \leq 1$, $K_t, K_r > 0$ and $K_{te}, K_{re} \geq 0$ are cutting parameters. The function $g_j\big(\phi_j(t)\big)$ describes whether a tooth is in or out of cut:

$$g_j\big(\phi_j(t)\big) = \begin{cases} 1, & \phi_s \leq \phi_j(t) \leq \phi_e \\ 0, & \text{else} \end{cases}. \tag{35}$$

After substitution of (1), (3) and (35), and summing for all teeth, equation (34) can be described in feed x- and normal y-direction as

$$\begin{aligned} \underline{F}(t) = a_p \sum_{j=0}^{z-1} g_j\big(\phi_j(t)\big) \Bigg(\Big(h_{j,\text{stat}}(t) + \\ \big[\sin\phi_j(t)\ \cos\phi_j(t)\big] \big(\underline{v}(t) - \underline{v}\big(t - \tau_j(t)\big)\big) \Big)^{x_F} \mathbf{S} \begin{bmatrix} K_t \\ K_r \end{bmatrix} + \\ \mathbf{S} \begin{bmatrix} K_{te} \\ K_{re} \end{bmatrix} \Bigg), \end{aligned} \tag{36}$$

with

$$\underline{F}(t) = \begin{bmatrix} F_x(t) \\ F_y(t) \end{bmatrix}, \quad \underline{v}(t) = \begin{bmatrix} v_x(t) \\ v_y(t) \end{bmatrix},$$
$$\mathbf{S} = \begin{bmatrix} -\cos\phi_j(t) & -\sin\phi_j(t) \\ \sin\phi_j(t) & -\cos\phi_j(t) \end{bmatrix}.$$

In (Insperger *et al.*, 2003), it is assumed to be possible to split the displacement $\underline{v}(t)$ into a $\hat{\tau}$-periodic displacement $\underline{v}_p$, which can be considered as the unperturbed tool motion when no self-excited vibrations arise, and a perturbation $\underline{v}_u$. The equation describing the periodic displacement does not include a delayed term since the period time is equal to the delay. In a next step, an equation for the perturbation is constructed by subtracting the periodic displacement from the total displacement. However, in the new model, due to the time dependent delay, $\underline{v}_p(t) - \underline{v}_p\big(t-\tau_j(t)\big) \neq 0 \forall t$. Therefore this term remains in the equation for the periodic displacement and hence in the equation of the perturbation. Unfortunately, the periodic displacement is unknown. Therefore, in order to overcome the existence of this delayed term a linear material model, i.e. $x_F = 1$, is assumed. Then, the forces due to the perturbation can be described as

$$\begin{aligned}\underline{F}_u(t) &= a_p \sum_{j=0}^{z-1} g_j\big(\phi_j(t)\big)\mathbf{S}\begin{bmatrix}K_t\\K_r\end{bmatrix}\big[\sin\phi_j(t)\ \cos\phi_j(t)\big] \\ &\quad \Big(\underline{v}_u(t) - \underline{v}_u\big(t-\tau_j(t)\big)\Big) \\ &= a_p \sum_{j=0}^{z-1} \mathbf{H}_j(t)\Big(\underline{v}_u(t) - \underline{v}_u\big(t-\tau_j(t)\big)\Big),\end{aligned} \tag{37}$$

with

$$\mathbf{H}_j(t) = g_j\big(\phi_j(t)\big)\mathbf{S}\begin{bmatrix}K_t\\K_r\end{bmatrix}\big[\sin\phi_j(t)\ \cos\phi_j(t)\big]\,. \tag{38}$$

Substitution of (37) as input $\underline{u}$ into (33) and realizing that $\underline{v}_u(t) = \underline{y}(t) = \mathbf{C}\underline{z}(t)$ (assuming $\mathbf{D} = \mathbf{0}$) gives

$$\begin{aligned}\dot{\underline{z}}(t) &= \mathbf{A}\underline{z}(t) + a_p \sum_{j=0}^{z-1} \mathbf{B}\mathbf{H}_j(t)\mathbf{C}\Big(\underline{z}(t) - \underline{z}\big(t-\tau_j(t)\big)\Big), \\ \underline{y}(t) &= \mathbf{C}\underline{z}(t).\end{aligned} \tag{39}$$

The semi-discretization method (Insperger and Stépán, 2004*a*; Insperger and Stépán, 2004*b*) can be used to determine the stability properties of systems of the form

$$\begin{aligned}\dot{\underline{z}}(t) &= \mathbf{P}(t)\underline{z}(t) + \sum_{j=0}^{z-1} \mathbf{Q}_j(t)\underline{z}\big(t-\tau_j(t)\big), \\ \mathbf{P}(t+T) &= \mathbf{P}(t), \quad \mathbf{Q}_j(t+T) = \mathbf{Q}_j(t),\end{aligned} \tag{40}$$

with T the period-time of the matrices $\mathbf{P}$ and $\mathbf{Q}_j$. The first equation in (39) is written in the form of (40) with

$$\mathbf{P}(t) = \mathbf{A} + a_p \sum_{j=0}^{z-1} \mathbf{B}\mathbf{H}_j(t)\mathbf{C}, \tag{41}$$

$$\mathbf{Q}_j(t) = -a_p \mathbf{B}\mathbf{H}_j(t)\mathbf{C}. \tag{42}$$

Since

$$\begin{aligned}\mathbf{H}_j(t+\hat{\tau})\mathbf{C}\underline{z}\big(t+\hat{\tau}-\tau_j(t+\hat{\tau})\big) = \\ \mathbf{H}_{j-1}(t)\mathbf{C}\underline{z}\big(t-\tau_{j-1}(t)\big),\end{aligned} \tag{43}$$

equation (39) is periodic with period time $\hat{\tau}$.

The choice whether the tool path is modelled as a circular arc or as a trochoid influences the delay, which is constant for the circular tool path and periodic for the trochoid tool path. Furthermore, the matrix $\mathbf{H}_j(t)$ changes as a result of the different entry and/or exit angles. However, the structure of the model as presented in equation (40) does not change. Therefore, the semi-discretization method can be used for both models.

3 Stability

In (Insperger and Stépán, 2004*b*) the semi-discretization method is demonstrated for a non-autonomous system with a constant delay. In (Insperger and Stépán, 2004*a*) the method was demonstrated for an autonomous system with a periodic delay. The milling model presented in section 2 is a non-autonomous system with multiple periodic delays. Using the semi-discretization method for this model is straightforward by combining the two cases mentioned in (Insperger and Stépán, 2004*b*) and (Insperger and Stépán, 2004*a*).

Whenever a mill is cutting, the tool experiences a displacement. This displacement is periodic with the tooth passing time $\hat{\tau}$ and is a result of the forces acting on the tool while cutting. In the model, this displacement is a periodic solution of (33) where the input $\underline{u}$ is the force described by (36). When no chatter occurs, this periodic solution is stable and when chatter occurs, it is unstable. Therefore, the chatter boundary can be found by regarding the stability of this periodic solution, which is assessed by considering the eigenvalues of the monodromy matrix.

The semi-discretization method gives a finite-dimensional approximation of the monodromy matrix $\mathbf{\Phi}$ over the principal period T. This period is divided in k equal intervals of length Δt. The approximation of the monodromy matrix is defined by

$$\underline{q}_k = \mathbf{\Phi}\underline{q}_0, \tag{44}$$

where $\underline{q}_k$ is a vector consisting of all the states $\underline{z}_i$ between the present and delayed time intervals. The periodic solution is locally stable (unstable) if the eigenvalues of the monodromy matrix, the so-called Floquet multipliers, are in modulus less (greater) than one.

Stability lobes have been generated using the traditional tool path model and the model presented in section 2. This has been done by point-by-point investigation of a grid in the parameter space consisting of the spindle speed Ω and depth of cut a_p. Herein, the resolution of the spindle speed is 50 rpm and the resolution

of the axial depth of cut is 0.25 mm. The dynamics of the spindle are modelled, in both x- and y-direction as a single linear mass-spring-damper system, as shown in figure 2, where

$$m\ddot{v}(t) + b\dot{v} + kv = m\ddot{v} + 2m\zeta\omega\dot{v} + m\omega^2 v. \quad (45)$$

The natural frequency of the system is defined by ω and the dimensionless damping by ζ. The parameters used in the model are $m_x = m_y = 0.02$ kg, $\zeta_x = \zeta_y = 0.05$, $\omega_x = \omega_y = 2\pi \cdot 2198$ rad, $K_t = 462$ N/mm$^{1+x_F}$, $K_r = 38.6$ N/mm$^{1+x_F}$, $x_F = 1$, $r = 5$ mm, $f_z = 0.15$ mm/tooth, $a_e = 0.5$ mm (=5%) and $k = 40$. The cutting parameters K_t, K_r are adopted from (Faassen *et al.*, 2003).

The stability lobes for up- and downmilling are shown in figure 9.

From this figure, it can be concluded that the differences between the stability lobes of both models increase if the radial immersion decreases. The error in the delay, as shown in figure 6, is the largest when the angle is close to 0 or π radians. Therefore, for a low immersion cut this error has a relatively large effect on the stability. Furthermore, the small difference in the entry and or exit angles shown in figure 5 has a relatively large effect for low immersion levels.

It can be seen that for the upmilling case, the peak of the stability lobes moves to the lower left if the new model is used instead of the traditional model. For the downmilling case, the peak moves to the lower right. The differences between up- and downmilling are relatively small for the traditional model. However, the differences in the new model are quite large, because the peaks move away from each other.

4 Discussion

When a stability lobe diagram is available in practice, most probably, a point beneath the lobe will be chosen at a certain distance from the stability border at a spindle speed where a peak in the SLD occurs. If the actual stability limit is shifted downward compared to the predicted limit, the chosen point may very well still be stable, since a certain safety margin was taken into account. However, a shift in the position of the lobes to the left or to the right may very well cause drastic changes in the stability of the chosen working point. If for example, for the mentioned parameter set and 5% immersion, the working point is chosen at 21550 rpm and $a_p = 66$ mm, the process is predicted to be stable in both up- and downmilling for the traditional model according to figure 9(4). At this spindle speed, the depth of cut can be increased with almost 20 mm. Therefore, the stability lobes can shift downwards with 20 mm, before the limit of stability is reached. However, when the same point is chosen for the trochoidal model according to figure 9(4), it is unstable for both up- and downmilling.

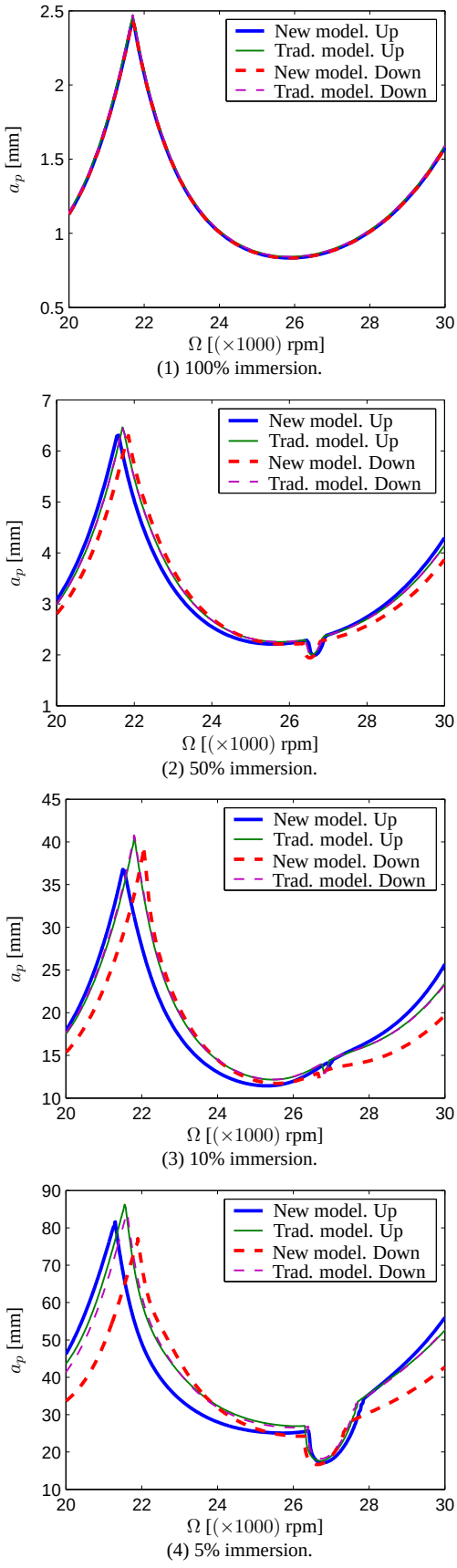

Figure 9: Stability lobes for up- and downmilling using the traditional and the new model for several immersion levels.

In order to explain the reason for the shift of the stability lobes using the new model, this model is analyzed further. The use of the new model results in three changes in the model compared to the traditional model. First, the static chip thickness takes a different shape as shown in figure 3. Next, the delay becomes a periodic function. Finally, the entry and exit angles change depending on whether we consider up- or downmilling. For a linear material model (i.e. $x_F = 1$), only the latter two changes influence the stability lobes. It is possible to retrieve the stability lobes while only one of these changes is taken into account. Of course, this temporary model is not representing an actual milling case, but is can be used to investigate the effects of these changes on the stability. For these models, the mentioned parameter set is chosen with a 5% immersion rate. First, the periodic delay is taken into account while the rest of the model is equal to the traditional model. The stability lobe for the downmilling case is shown in figure 10(1). As can be seen, the lobe moves to the right. If the delay is taken constant while the exit angle is changed according to the new model, the stability lobes move downwards as is shown in figure 10(2).

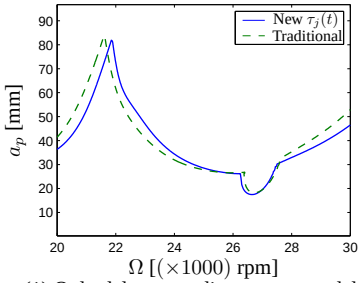

(1) Only delay according to new model.

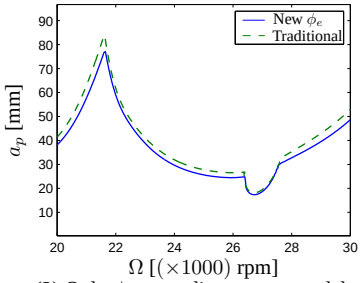

(2) Only ϕ_e according to new model.

Figure 10: Stability lobe for 5% downmilling using the traditional and parts of the new model.

Hence, it can be concluded that the shift to the right of the lobe in figure 9(4) is caused by the periodic delay. This can be explained as follows. Chatter is caused by vibrations of the cutter on the tooth path. In one tooth pass period, $N + \epsilon$ waves exist on the workpiece where N is the number of full waves and $\epsilon < 1$ the fraction of incomplete waves, see the upper part of figure 11.

If the lobe of an SLD is followed from left to right for a system with a single natural frequency, the fraction ϵ of these waves decreases as is shown in figure 12. At the peak of a lobe, a jump is made to a wave where N is decreased by one, e.g. the number of waves goes from 3.2 to 2.8.

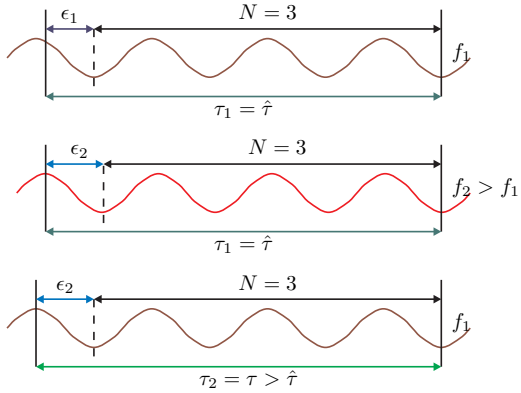

Figure 11: Effect of the frequency change $f_1 \rightarrow f_2$ and the delay change $\tau_1 \rightarrow \tau_2$ on the fraction of waves ϵ_1 and ϵ_2.

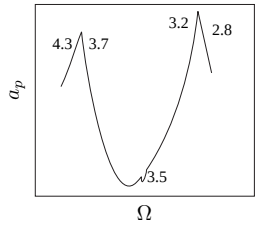

Figure 12: Stability lobe with some possible values for the number of waves $N + \epsilon$.

If the natural frequency of the system increases, more waves are generated in the tooth path for the same spindle speed, see the middle part of figure 11. This will cause the stability lobes to move to the right, since for the same spindle speed the fraction ϵ is increased.

For downmilling at 5%, the angles at which the cutter is engaged, lie close to π. As can be seen in figure 6, this gives a delay of about 1-1.5% higher than the constant delay $\hat{\tau}$. Therefore, the interval $t - \tau_j(t)$ is 1-1.5% larger than the interval $t - \hat{\tau}$, which allows 1-1.5% more waves to exist within this interval. This is depicted schematically in the lower part of figure 11.

Therefore, the stability lobes using this periodic delay show some resemblance with lobes generated using machine dynamics with a 1% higher natural frequency, while the stiffness is kept at the old value. These lobes are shown in figure 13. Using this higher natural frequency causes the peaks of the lobe to move to the right, which is also the case for downmilling with the new model.

The peaks of the proposed model also shift downwards, as a result of the changed exit angle, in case of down milling. This is due to the fact that the tooth is longer in cut, so the average force over one tool revolution is increased.

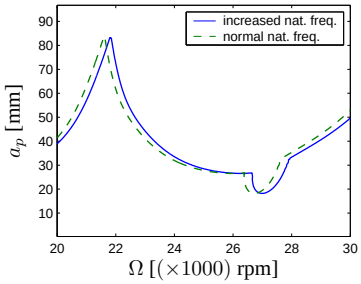

Figure 13: Stability lobe for 5% downmilling using the traditional model with the original and a 1% higher natural frequency.

5 Conclusions

Traditionally the tool path of a non-vibrating mill is modelled as a circular arc. In practice, the tool path is a trochoid. In modelling the milling process, this has consequences for the static chip thickness, the delay and the entry and/or exit angles. Equations for the static chip thickness, the periodic delay and the entry and exit angles have been derived. These models are more accurate than the models traditionally used.

An updated milling model has been constructed using these new equations. For the sake of simplicity, a linear material model is used. The limit of stability of the traditional model is compared to the limit of stability of the new model. Hereto, the semi-discretization method is used for several radial immersion levels for both up- and downmilling. It was found that using the new model for low radial immersion cuts, the peaks of the SLD move to the lower right for downmilling and to the lower left for upmilling compared to the traditional model. This is mainly caused by the periodic delay. For higher radial immersion rates, the differences between the two models decrease.

From simulation results, it appears that for accurate prediction of the stability lobes for low-immersion cutting it is necessary to drop the assumption that the tooth path is a circular arc. The tooth path should be modelled as a trochoid. In the future, the stability lobes of both models should be validated by performing dedicated experiments.

Acknowledgements

This research is part of the TNO project Chattercontrol, which is supported in part by Jabro Tools, Philips ETG, Plasdan-Metaco and Somatech.

References

Altintas, Y. (2000). *Manufacturing automation*. Cambridge University Press.

Altintas, Y. and E. Budak (1995). Analytical prediction of stability lobes in milling. *Annals of the CIRP* **44**(1), 357–362.

Davies, M.A., B. Dutterer and J.R. Pratt (2002). Device for stable speed determination in machining. US patent no. 6,349,600.

Faassen, R.P.H., N. van de Wouw, J.A.J. Oosterling and H. Nijmeijer (2003). Prediction of regenerative chatter by modelling and analysis of high-speed milling. *International Journal of Machine Tools and Manufacture* **43**(14), 1437–1446.

Insperger, T. and G. Stépán (2004*a*). Stability analysis of turning with periodic spindle speed modulation via semi-discretization. *Journal of Vibration and Control* **10**, 1835–1855.

Insperger, T. and G. Stépán (2004*b*). Updated semi-discretization method for periodic delay-differential equations with discrete delay. *International Journal for Numerical Methods in Engineering* **61**(1), 117–141.

Insperger, T. and G. Stépán (2004*c*). Vibration frequencies in high-speed milling process or a positive answer to Davies, Pratt, Dutterer and Burns. *Journal of Manufacturing Science and Engineering, Transactions of the ASME* **126**(3), 481–487.

Insperger, T., G. Stépán, P.V. Bayly and B.P. Mann (2003). Multiple chatter frequencies in milling processes. *Journal of Sound and Vibration* **262**(2), 333–345.

Li, H.Z., K. Liu and X.P. Li (2001). A new method for determining the undeformed chip thickness in milling. *Journal of Materials Processing Technology* **113**, 378–384.

Martellotti, M.E. (1941). An analysis of the milling process. *Transactions of the ASME* **63**, 677–700.

Martellotti, M.E. (1945). An analysis of the milling process. part 2. down milling. *Transactions of the ASME* **67**, 233–251.

Spiewak, S. (1994). Analytical modeling of cutting point trajectories in milling. *Journal of Engineering for Industry, Transactions of the ASME* **116**, 440–448.

Spiewak, S. (1995). An improved model of the chip thickness in milling. *Annals of the CIRP* **44**(1), 39–42.

Szalai, R., G. Stépán and S.J. Hogan (2004). Global dynamics of low immersion high-speed milling. **14**(4), 1069–1077.

Tlusty, J. and M. Polacek (1963). The stability of machine tools against self-excited vibrations in machining. In: *Proceedings of the ASME International Research in Production Engineering Conference*. Pittsburgh, USA.

Tobias, S.A. and W. Fishwick (1958). The chatter of lathe tools under orthogonal cutting conditions. *Transactions of the ASME* **80**, 1079–1088.